TU Delft

Delft University of Technology

Assessing historical church tower asymmetry using point cloud spatial expansion

Dabrowski, Pawel S.; Zienkiewicz, Marek Hubert; Truong-Hong, Linh; Lindenbergh, Roderik

DOI
10.1016/j.jobe.2023.107040

Publication date
2023

Document Version
Final published version

Published in
Journal of Building Engineering

Citation (APA)
Dabrowski, P. S., Zienkiewicz, M. H., Truong-Hong, L., & Lindenbergh, R. (2023). Assessing historical church tower asymmetry using point cloud spatial expansion. *Journal of Building Engineering*, *75*, Article 107040. https://doi.org/10.1016/j.jobe.2023.107040

Important note
To cite this publication, please use the final published version (if applicable).
Please check the document version above.

Copyright
Other than for strictly personal use, it is not permitted to download, forward or distribute the text or part of it, without the consent of the author(s) and/or copyright holder(s), unless the work is under an open content license such as Creative Commons.

Takedown policy
Please contact us and provide details if you believe this document breaches copyrights.
We will remove access to the work immediately and investigate your claim.

This work is downloaded from Delft University of Technology.
For technical reasons the number of authors shown on this cover page is limited to a maximum of 10.

Green Open Access added to TU Delft Institutional Repository

'You share, we take care!' - Taverne project

https://www.openaccess.nl/en/you-share-we-take-care

Otherwise as indicated in the copyright section: the publisher is the copyright holder of this work and the author uses the Dutch legislation to make this work public.

Journal of Building Engineering 75 (2023) 107040

Contents lists available at ScienceDirect

Journal of Building Engineering

journal homepage: www.elsevier.com/locate/jobe

Assessing historical church tower asymmetry using point cloud spatial expansion

Pawel S. Dabrowski [a,*], Marek Hubert Zienkiewicz [b], Linh Truong-Hong [c], Roderik Lindenbergh [c]

[a] Department of Geodesy and Oceanography, Gdynia Maritime University, Sedzickiego 19, 81-374, Gdynia, Poland
[b] Department of Geodesy, Gdansk University of Technology, Narutowicza 11/12, 80-233, Gdańsk, Poland
[c] Department of Geoscience and Remote Sensing, Delft University of Technology, Stevinweg 1, 2628, CN Delft, the Netherlands

ARTICLE INFO

Keywords:
Historical buildings
Asymmetry
Prismatic PCSE

ABSTRACT

Church towers are key cultural heritage. In theory, towers are vertical, while facade elements are symmetrically positioned around the tower axis. However, during service of a structure, building and lifetime conditions cause deviations, with associated risks. Laser scanning point clouds can be used to assess the structural state but a universal approach was missing. The proposed algorithm first estimates the tower inclination, and tests which multi-axis representation best represents the course of the tower. Next, point cloud spatial expansion recovers relative distances and deviations of facade elements. The resulting procedure was applied to assess two Dutch medieval towers including the Old Church in Delft and the St. Bavo Church in Haarlem, respectively. As results of analysis, significant asymmetry was found with a 1.4° deviation of the multi-modal axis of the St. Bavo Church tower together with variations of 0.1%–1.5% for facade slopes, while 0.1°–3.1° radial deviations were found in the position of the turrets of the Old Church tower.

1. Introduction

The goal of the study is to assess conditional status of structures having an idealized symmetrical, regular geometry. This is an important step in maintenance and operation of the structure. The factors that are monitored include to determine the local stability of the surface shape [1], identify the occurrence of cracks and damages [2]. Also, the processes related to the entire structure, e.g. a tilt of the structure can be monitored [3]. The results of processed measurements may imply actions preventing the disturbances in the exploitation of the structure [4]. Periodic monitoring of structures in the long term enables determining the trend of asymmetric changes in shape, e.g., bending the axis of symmetry of the structure. Both symmetrical masonry [5], and steel [6] structures are subject to geometric assessment. A related category of analysis is the assessment of the regularity and symmetry of objects with a known cross-section [7]. The factor of structure inclination was also faced from the structural point of view considering the stability of the structure against possible increments of inclination [8].

Electro-optical methods as terrestrial laser scanning (TLS) and total station systems have been used to capture geometry of a structure to assess their condition [9,10]. One of the advantages of these measurement methods is to provide high accuracy and the large amount of discrete points representing detailed surfaces of the structures. Additionally, photogrammetric methods are also used to capture the geometric information of structures [11,12], whose metrological comparison with laser technology was presented by

* Corresponding author.
E-mail address: p.dabrowski@wn.umg.edu.pl (P.S. Dabrowski).

https://doi.org/10.1016/j.jobe.2023.107040
Received 12 April 2023; Received in revised form 29 May 2023; Accepted 7 June 2023
Available online 8 June 2023
2352-7102/© 2023 Elsevier Ltd. All rights reserved.

Aldao et al. [13]. Point clouds are then used to conduct geometric analysis in the three-dimensional (3D) model space [14], to create their expansions [15], or to use for a finite element model (FEM) analysis [16].

Point clouds are also used in block-based computational analysis of historical masonry structures, e.g. Pereira et al. presented the method of nonperiodic block-by-block pattern generation to assess the structure of historical buildings using voxels [17]. A related study involving the application of point clouds on multi-leaf nonperiodic masonries was presented by Bartoli et al. [18]. To reproduce a reliable numerical model of masonry towers, two non-destructive identification techniques, Experimental and Operation Modal Analyses, were introduced by Standoli et al. [19]. Their experiment involved vibrational monitoring of structures to assess a building's behavior to evaluate the seismic risk or other possible interventions. The impact of the friction coefficient on the mechanical response of a tower undergoing seismic actions using the Non-Smooth Contact Dynamics method was studied by Ferrante et al. [20].

Most well-known approaches used to assess the conditional state of structures are based on as-design models with common primitive objects, for example a cylinder and sphere, while neglecting the irregularities in the objects' element of symmetry. Ye et al. [21] used a cylinder to assess a freemason arch bridge, while Lenda et al. [22] assessed a thin-walled dome by assuming its shape as a sphere. Objects of a more complex shell shape are examined, among others, by using spline functions, Kriging, or Fourier series [23]. An important factor taken into account is the inclination of the structure from the vertical [24], which is related to the object's axis. The symmetry elements used in those studies, e.g. one straight line defining the axis of a cylindrical object do not cover cases with objects of more complex irregular geometry. However, after long service, the structure is subjected to deterioration, in which the shape of the structure significantly differs from as-design model. As such, the methods-based common primitive objects may give relatively low accuracy of the structure deformation. That requires an appropriate method to be developed to assess deformed or irregular shape of the structure.

The motivation for this study was to extend the scope of geometry analyses by determining the asymmetry parameters of inclined historical symmetrical objects with an atypical course of the axis of symmetry. Two medieval church towers, the Old Church in Delft and the St. Bavo Church in Haarlem in the Netherlands, were used as a case study. The first is a square tower, and the second is an octagonal tower. In this study, a novel asymmetry assessment method known as the point cloud spatial expansion (PCSE) is proposed to enable assessment of prismatic objects with a discontinuous surface course. An important innovative factor in this study is the formulation of the functions of the prismatic PCSE such that the irregular course of the tower axis is taken into account.

The research problem of the study was the formulation of a universal algorithm of asymmetry assessment applicable to historical towers. Both the position and the modularity of the object's axis of symmetry were taken into account in the analysis process. The algorithm defines the asymmetry properties of walls, story levels, and additional architectural elements of the structure by eliminating the influence of the axis inclination factor. The study aims to determine the axis of symmetry of historical church towers. The irregular shape of the towers may cause the axis of symmetry to break into a polyline. Subsequently, the deviations of symmetry of facade elements at different height with respect to the estimated axis of symmetry of the tower is assessed.

The paper is divided into four sections. After the introduction with the state-of-the-art and research motivation, the second section describes the case studies while the proposed method presents in the following section. Next, results of the analyses are presented while discussions and conclusions are presented in the last section.

2. Case studies

Two medieval church towers, the Old Church in Delft and the St. Bavo Church in Haarlem in the Netherlands, were used as a case study. Both towers were sampled by a Leica ScanStation P40 scanner. The resulting point clouds (Fig. 1) of the church medieval towers in Delft (52° 0 '45.3 "N, 4° 21' 19.5" E) and Haarlem (52° 22 '51.9 "N, 4° 38' 14.1" E) are available at the repository 4TU.ResearchData TU Delft [25,26]. The first tower was built in 1325, and the second was built in 1520 and renovated in 1969. In the first step, point cloud registration was assessed, and after determining the transformation parameters, the position of the point cloud components was corrected. The characteristic features of the tested objects are regular polygon cross-sections (square in the case of the tower in Delft, octagon in the case of the tower in Haarlem), and the inclination of the structures from the vertical. The church tower in Delft has four

Fig. 1. The Old Church in Delft (left panels), and the St. Bavo's Church in Haarlem (right panels) tower pictures and point clouds.

side-towers (turrets) on top, is made of brick and is 75 m high. The church tower in Haarlem is made of wood, covered with lead, and reaches 78 m.

The Delft tower was added to the church in the direct vicinity of an old canal. As a consequence, the foundations did not properly support the building. After the stabilization of the structure, the construction was continued at the time with compensation for the tower tilt [27]. The Haarlem tower originally was built as a masonry structure, however, due to the tilting of the tower pillars and wall cracks occurrences, it was decided to change it to a wooden tower. The timber support of the tower is covered with lead cladding, like the rest of the church roof. A chemical reaction between the lead and the acetic acids in timber Oakwood caused corrosion. This factor, connected with the quality of the medieval workmanship, caused cracks and leakage towards the timber. The other source of timber damage is insects [28]. The cause of the inclination of the Haarlem wooden tower is unknown, however, the purposeful explanation is to provide withstand the tower from the north-eastern wind [29].

3. Methods

The presented methodology enables the assessment of objects' regularity and symmetry by determining the multi-modal axis of symmetry and using its parameters in the process of point cloud verticalization [30]. Based on the processed point cloud, a spatial expansion, an alternative form of object structure presentation, is created. The new factor is the introduction in the PCSE method of the prism geometry as a principal reference to the analyzed point cloud. Earlier studies [3,29] defined the parameters of the Haarlem St. Bavo Church tower inclination and slopes of the facades. The novel approach proposed in this study is to recreate the axes' collinearity on all levels of a tower and then evaluate its initial symmetry parameters based on a discrete representation of the axis given by estimated on-axis points. Also, the deviations of the individual levels of the tower and the parameters of the surfaces of the walls were determined.

The principal shapes of the two towers are regular prisms: square and octagonal, which are used as reference models in geometric analysis. The point cloud spatial expansion (PCSE) method was used to assess the parameters of asymmetry and regularity of objects' elements. The original PCSE [15] was only applied for cylinder-based objects, and is not applicable for prismatic towers. However, the approach of estimation of symmetrical objects' axes inclination described in Refs. [30,31] is also applied in this study to estimate polyline axis. The historical prismatic towers asymmetry algorithm covers estimation of axis of symmetry, elimination of axis inclination factor, point cloud spatial orientation, partitioning, and PCSE expansion (Fig. 2). The results of subsequent algorithm stages are used in assessment of asymmetry of the tower.

The consecutive three stages (I, II, and III) of the algorithm are presented in Subsections 3.1, 3.2, and 3.3. The contribution of the proposed application of the PCSE method are the discontinuous course of the prismatic objects' surfaces and the introduction of the radial partitioning of the verticalized point cloud. After the point cloud partitioning, the prismatic spatial expansion is performed. No surrogate models of two towers were used in the examination, as the PCSE method involves a comparison of the real shape of the measured structure to the adopted reference solid of a prism.

3.1. Symmetry axis estimation (Stage I)

The procedure of axis estimation presents in three steps. The first step is to extract the wall planes from the point cloud using the Random sample consensus (RANSAC) method [32], and extract cross-sections perpendicular to the direction of the walls of the building. In the second step, the coordinates of the centers of the cross-sections indicating the axis course are determined. In the third step, the axis of the tower symmetry is estimated from the center points.

3.1.1. Cross-sections extraction

The position of the axis of assumed symmetrical objects is not directly available in point clouds. Only parts of the object's surface are measured. The tower's general geometry of major walls is defined by cross-sections' shape, and centers of the sections that represent the course of the object's axis of symmetry. As such, these centers must be estimated. A set of centers of the cross-section extracted at different heights of the tower is assumed to represent the tower axis. In case of the two towers analyzed here, the axis

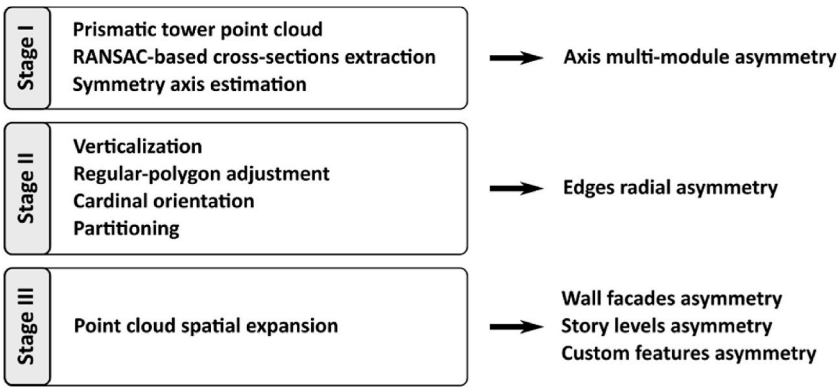

Fig. 2. Algorithm of historical prismatic towers asymmetry assessment used in the study.

inclination factor was taken into account in extracting the point cloud of the cross-sections, which were selected in a plane perpendicular to the course of the tower walls.

An irregular structure shape can cause difficulty in estimating the axis parameters. This factor is particularly important for the Haarlem St. Bavo Church tower with numerous architectural features. In the case of circular cross-sections of cylindrical objects, robust estimation methods were used to eliminate outliers from the set of points [33]. used the Huber damping function, and Nurunnabi et al. [34] Huber [35] used robust principal components in the estimation of the centers of circular sections. In this study, cross-sections of both towers are respectively of squared and octagonal shape (Fig. 3). To exclude irrelevant points (including outliers), the RANSAC method [32]was used to extract data points of surfaces representing towers' wall panels. Two conditions were taken into account in the selection of planes. The first one was the area of the point cloud covered by the estimated RANSAC plane. The second one was compliance of the estimated planes with the reference solid, as points of the selected parts of the cloud in the next stage were used to estimate the local direction of the inclined tower symmetry axis.

After the elimination of outliers and redundant points by RANSAC, the point cloud subsets describing tower walls were used to extract the cross-sections. Due to the towers' inclination, horizontal-plane extraction was not justified in cross-section extraction, as it would generate errors in estimating the center of a cross-section. Hence, the walls-perpendicular method of section extraction was applied. The number and the thickness of the cross-sections selected depend on the shape of the object and the quality of the point cloud. For the Delft Old Church tower, the cross-section extraction was limited by partial point cloud representation of the object's rear walls (left panel Fig. 3). A similar wall-based approach of cross-section extraction was used for the Haarlem St. Bavo tower. The Haarlem tower facades were obscured by numerous wooden ornaments and architectural features. Also, the shape of facades' planes varied, e.g., the facade plane on the top levels of the tower were represented only by narrow vertical fragments (right panel Fig. 3).

In this study, eleven and twelve cross-sections were used to determine the axis of the tower of the Delft Old Church and the St. Bavo Church, respectively, in which the section thickness was 5 mm. Sections thickness and localization resulted from the quality of the towers' point clouds. The factor of non-horizontal cross-sections' configuration needed to be eliminated in the center points estimation, which was achieved by using principal component analysis (PCA) [36] to bring the sections to a temporary horizontal plane:

$$\boldsymbol{P}^{'} = \boldsymbol{R}\left(\boldsymbol{P} - \boldsymbol{P}_0^{PCA}\right) + \boldsymbol{P}_0^{PCA}, \tag{1}$$

where $\boldsymbol{P}^{'}$ denotes the horizontal equivalent of a point $\boldsymbol{P}$ from the cloud, and $\boldsymbol{P}_0^{PCA}$ denotes the point on the estimated cross-section plane. The term $\boldsymbol{R}$ denotes the cumulative matrix of elementary rotations $\boldsymbol{R_Y}$ and $\boldsymbol{R_Z}$ with angles $\alpha = atan\,2(V_x^{PCA}, V_y^{PCA})$ and $\beta = acos(\sqrt{V_x^{PCA\,2} + V_y^{PCA\,2}}\,/|\boldsymbol{V}^{PCA}|)$ obtained from the formula:

$$\boldsymbol{R} = \boldsymbol{R_Z}(-\alpha)\boldsymbol{R_Y}\left(\pi/2 - \beta\right)\boldsymbol{R_Z}(\alpha), \tag{2}$$

where $\boldsymbol{V}^{PCA}$ denotes the estimated cross-section plane normal vector.

3.1.2. Center points estimation

The transformed points $\boldsymbol{P}^{'}$ of each cross-section are used to estimate the center in the following steps. The first step is the determination of four or eight lines representing the sides of the square or octagon, respectively. RANSAC applied to points of tower walls' subsets was used to identify points representing all sides (cf. Fig. 3). Adaptation of the same height for all points in the cross-sections

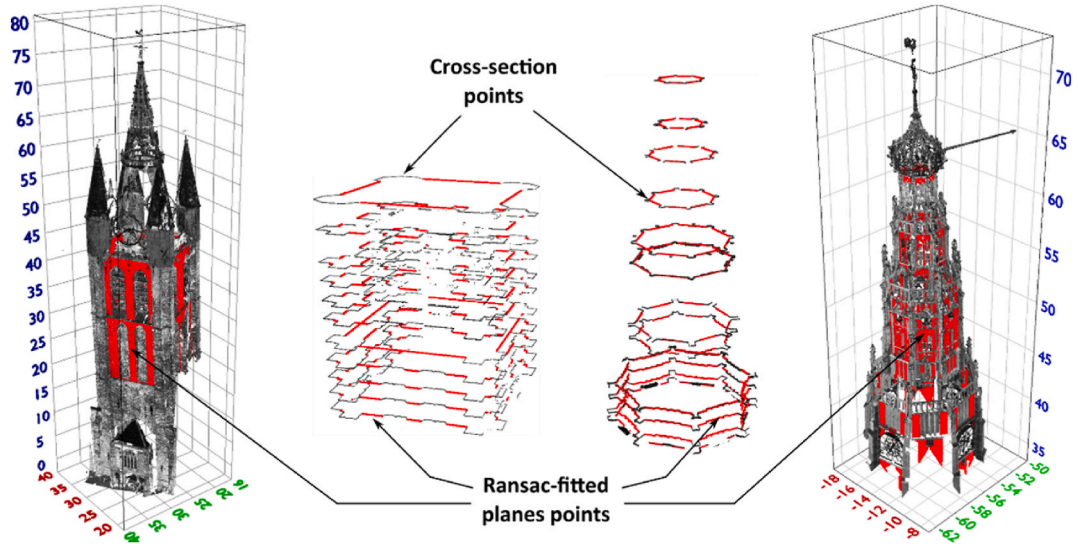

Fig. 3. Square and octagonal towers' point cloud cross-sections.

enabled performing a line fit in $\mathscr{R}^2$ due to the cross-section thickness factor. The lines given by the slope a_i and y-intercept b_i represent the figure sides on the reference prism faces. The second step is to estimate the coordinates x and y, and the coordinate errors m_x, m_y of four and eight vertices of the polygon $\boldsymbol{P}_X$, respectively:

$$\boldsymbol{P}_X = [x \quad y]^T = \left[\frac{b_l - b_k}{a_k - a_l} \quad \frac{a_l \bullet b_k - a_k \bullet b_L}{a_l - a_k}\right]^T, \tag{3}$$

$$m_x = \frac{1}{|a_k - a_l|}\sqrt{x^2\left(m_{a_k}^2 + m_{a_l}^2\right) + m_{b_k}^2 + m_{b_l}^2}, \tag{4}$$

$$m_y = \frac{1}{|\mathrm{a_k} - \mathrm{a_l}|}\sqrt{x^2\left(a_l^2 m_{\mathrm{a_k}}^2 + a_k^2 m_{\mathrm{a_l}}^2\right) + \mathrm{a_l}^2 m_{\mathrm{b_k}}^2 + a_l^2 m_{\mathrm{b_k}}^2 + \mathrm{a_k}^2 m_{\mathrm{b_l}}^2}, \tag{5}$$

where vertex point $\boldsymbol{P}_X$ denotes the intersection of lines $k : f(x) = a_k x + b_k$ and $l : f(x) = a_l x + b_l$, and $m_{\mathrm{a_k}}$, $m_{\mathrm{b_k}}$, $m_{\mathrm{a_l}}$, and $m_{\mathrm{b_l}}$ denote errors of two line parameters determined using Gaussian error propagation [37]. In the calculation uniform point precision was assumed.

Results of fitting straight lines from the point cloud of the cross-sections and the position of the calculated polygons' vertices are presented in Fig. 4.

In the third step, the vertex coordinates were used to determine slope a and y-intercept b of the polygon diagonals (cf. Fig. 5). The coefficients errors m_a and m_b of a line passing through two given points $\boldsymbol{P}_1$ and $\boldsymbol{P}_2$ were determined using the formulas:

$$m_a = \frac{1}{x_{\boldsymbol{P}_2} - x_{\boldsymbol{P}_1}}\sqrt{a^2\left(m_{x_{\boldsymbol{P}_1}}^2 + m_{x_{\boldsymbol{P}_2}}^2\right) + m_{y_{\boldsymbol{P}_1}}^2 + m_{y_{\boldsymbol{P}_2}}^2}, \tag{6}$$

$$m_b = \frac{1}{|x_{\boldsymbol{P}_2} - x_{\boldsymbol{P}_1}|}\sqrt{x_{\boldsymbol{P}_1}^2\left(a^2 m_{x_{\boldsymbol{P}_2}}^2 + m_{y_{\boldsymbol{P}_2}}^2\right) + x_{\boldsymbol{P}_2}^2\left(a^2 m_{x_{\boldsymbol{P}_1}}^2 + m_{y_{\boldsymbol{P}_1}}^2\right)}. \tag{7}$$

The center $\boldsymbol{C}'$ of the cross-section were determined using ordinary least-squares (OLS):

$$\boldsymbol{C}' = \left(\boldsymbol{A}^T \boldsymbol{W} \boldsymbol{A}\right)^{-1}\left(\boldsymbol{A}^T \boldsymbol{W} \boldsymbol{y}\right), \tag{8}$$

where $\boldsymbol{A} = \begin{bmatrix} a_1 & -1 \\ \vdots & \vdots \\ a_n & -1 \end{bmatrix}$ denotes the model Jacobian matrix, $\boldsymbol{W} = diag(m_{a_n}^{-2})$ is the matrix of weights calculated according to the estimated diagonal coefficient errors, and $\boldsymbol{y} = [-b_1 \quad \cdots \quad -b_n]^T$ denotes the vector of diagonals' y-interceptions. An example result of the estimation is presented in Fig. 5. The intersection estimate **C'** of four diagonals is denoted by red star symbol. Estimation error in the bottom-right corner is denoted by mP.

In the last step, the reverse transformation from the temporary horizontal plane to the original inclined plane of the cross-section was performed. The estimator $\boldsymbol{C}'$ has a z-coordinate value corresponding to the averaged z-coordinate of the data points of the cross-section. Thus, the center C of the cross-section in the original point cloud was obtained using Eq. (9):

$$\boldsymbol{C} = \boldsymbol{R}^{-1}\boldsymbol{C}' + \boldsymbol{P}_0^{PCA}. \tag{9}$$

3.1.3. Axis determination

The above procedure was applied on point clouds of each cross-section to determine a set of consecutive centers of the cross-section, which represent the towers' axes. The single-line segment axes parameters in $\mathscr{R}^3$ were determined using the PCA method. Next, the multi-modal polyline axis was created based on single-line elements. An equivalent method to use is the total least-squares estimation approach proposed in Ref. [38]. In both cases, the line-segment in a parametric form is used (Eq. (10)):

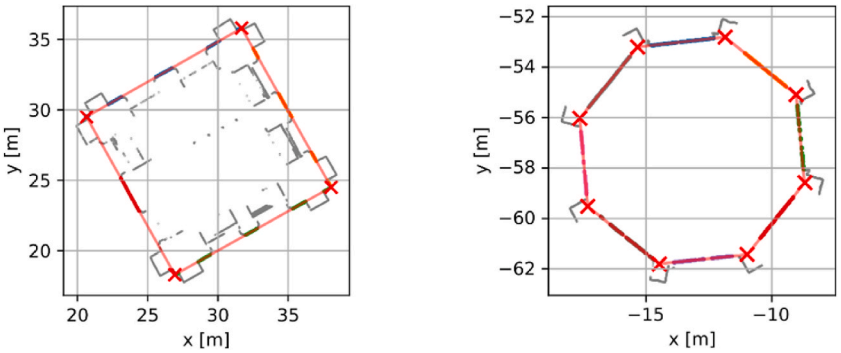

Fig. 4. Estimated vertices and sides of square (left), and octagonal (right) polygons of two horizontal cross-sections.

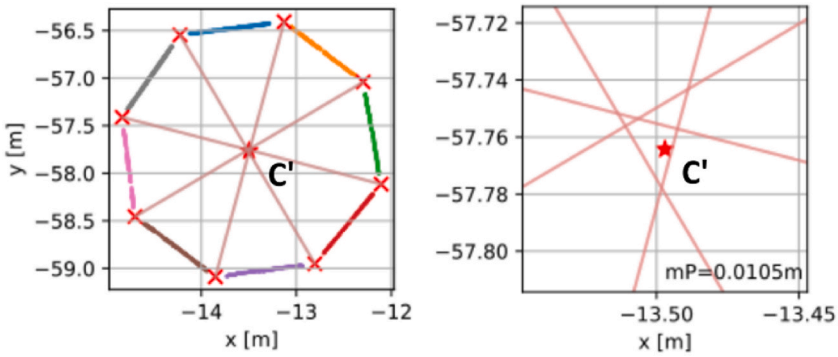

Fig. 5. Estimate a center point of an octagonal horizontal cross-section.

$$\boldsymbol{l}(t) = \boldsymbol{P}_{l_{mid}} + t \bullet \boldsymbol{V}_l, \tag{10}$$

where $\boldsymbol{P}_{l_{mid}}$ denotes a point on the line, $\boldsymbol{V}_l$ is the directional vector of the line, and t denotes the along-line scaling parameter.

For the Haa rlem St. Bavo tower, a discontinuous course of the axis of symmetry, changing with the objects' story levels was obtained. Taking into account the irregular shape of the axis, the fitting of a tower axis can be applied to either the full set of center points or the subsets representing tower stories. The literature describes the determination of a set of competing estimators using the M_{split} method [39,40], e.g., fitting number of line segments in one two-dimensional point dataset. In the considered case, the performed analysis indicated introducing several modules of the symmetry axis for separate levels of the tower estimated using PCA. The analysis is described in detail in the Results section.

Assuming the modular structure of the axis of symmetry, as it was stated for the Haarlem St. Bavo tower, the determination of the vectors of axis shifts between the successive levels was required to define its course on all tower levels. The shift vectors between the consecutive tower levels i and j were denoted $\boldsymbol{U}_{i,j}$. The boundary level heights were determined empirically due to the lack of representation of the wooden tower floors in the measured TLS point cloud. The coordinates of the temporary point $\boldsymbol{P}_{\mathbf{G}_{i,j}}$ on the boundary level were calculated as average values of the cross-section points. Determination of the coordinates of the shift vector $\boldsymbol{U}_{i,j}$ required indicating points on two symmetry axes of adjacent levels. The value of the parameter t defining the projection of a temporary point on each axis is obtained by the formula:

$$t_{\boldsymbol{P}_{\mathbf{G}_{i,j}}} = \left(x_V\left(x_{\boldsymbol{P}_0} - x_{\boldsymbol{P}_{\mathbf{G}_{i,j}}}\right) + y_V\left(y_{\boldsymbol{P}_0} - y_{\boldsymbol{P}_{\mathbf{G}_{i,j}}}\right) + z_V\left(z_{\boldsymbol{P}_0} - z_{\boldsymbol{P}_{\mathbf{G}_{i,j}}}\right)\right) \Big/ |\boldsymbol{V}|^2, \tag{11}$$

where x_V, y_V, z_V denote the line directional vector $\boldsymbol{V}$ coordinates, $x_{\boldsymbol{P}_0}, y_{\boldsymbol{P}_0}, z_{\boldsymbol{P}_0}$ denote coordinates of point $\boldsymbol{P}_0$ defining the line course, and $x_{\boldsymbol{P}_{\mathbf{G}_{i,j}}}, y_{\boldsymbol{P}_{\mathbf{G}_{i,j}}}, z_{\boldsymbol{P}_{\mathbf{G}_{i,j}}}$ denote the temporary point coordinates.

The shift vector between two axes of successive structure levels i and j is calculated using Eq. (12):

$$\boldsymbol{U}_{i,j} = \boldsymbol{P}_{\Delta_j} - \boldsymbol{P}_{\Delta_i}, \tag{12}$$

where $\boldsymbol{P}_{\Delta_i}$ and $\boldsymbol{P}_{\Delta_j}$ denote the on-axis projections of the temporary point $\boldsymbol{P}_{\mathbf{G}_{i,j}}$ on the boundary plane between the i-th and j-th tower levels.

The multi-modal axis of symmetry is defined by a set of lines parameters (Eq. (10)) and shift vectors (Eq. (12)) determined on the successive boundary levels of the tower. The axis parameters were used in the next stage of the study for point cloud verticalization and partitioning.

3.2. Tower point cloud partitioning (Stage II)

Partitioning aims to define several radially-defined point cloud subsets corresponding to different facade orientations that will form parts of the PCSE expansion. The number of subsets is respectively four (the Delft tower) or eight (the Haarlem St. Bavo tower) sides of the basis of the reference prisms of towers. The deviation of the towers' symmetry axes from the vertical is an obstacle for point cloud partitioning because of the structure inclination. The parameters of the axis of symmetry determined in Section 3.1 are used to eliminate the inclination factor. The transformed point cloud is constructed in a first step such that it has a linear vertical axis of symmetry and is located at the origin of the coordinate system. In the second step, based on the coordinates of the vertices calculated in Subsection 3.1.2, the adjusted directions of the regular polygons are determined. Then, the point cloud is transformed to a position corresponding to the orientation of the walls in relation to corresponding sides of the tower, for example the four sides of the world (North, East, South and West) of the Old Church in Delft. Finally, the partitioning of the verticalized point cloud with a cardinal orientation was performed, which is a condition for the application of the PCSE method.

3.2.1. Verticalization

The verticalization of point clouds is performed according to Eq. (13):

$$\boldsymbol{P}^{'} = \begin{cases} \boldsymbol{R}_Z(-\alpha_i)\cdot\boldsymbol{R}_Y\left(\pi/2-\beta_i\right)\cdot\boldsymbol{R}_Z(\alpha_i)\cdot\left(\boldsymbol{P}-\boldsymbol{P}_0^i\right)^T & for \quad i=1 \\ \boldsymbol{R}_Z(-\alpha_i)\cdot\boldsymbol{R}_Y\left(\pi/2-\beta_i\right)\cdot\boldsymbol{R}_Z(\alpha_i)\cdot\left(\boldsymbol{P}-\boldsymbol{P}_0^i\right)^T+\boldsymbol{U}_{i,i-1} & for \quad i>1 \end{cases}, \tag{13}$$

where $\boldsymbol{P}^{'}$ denotes the point in the verticalized point cloud, $\boldsymbol{P}_0^i$ and $\boldsymbol{V}^i$ are respectively the point and the vector defining the symmetry axis segment, i is the number of the axis module, $\alpha = atan\,2(\boldsymbol{V}_x^i, \boldsymbol{V}_y^i)$ and $\beta = acos(\sqrt{\boldsymbol{V}_x^{i\,2}+\boldsymbol{V}_y^{i\,2}}\,/|\boldsymbol{V}^i|)$ denote the rotation angles, $\boldsymbol{P}$ denotes the point in the original point cloud, and $\boldsymbol{U}_{i,i-1}$ denotes the shift vector between the adjacent tower levels.

Objects with one axis of symmetry, here the Delft Old Church tower, require only the first conditional formula from the verticalization equation. Objects with a multi-module axis of symmetry, here the tower in Haarlem, require in addition the shift vectors $\boldsymbol{U}_{i,j}$ to incorporate the changing inclination on the axis course. The comparison of the original and verticalized point clouds is shown in Fig. 6.

The figure illustrates the tower point clouds in an orthogonal top view. Fig. 6a and **c** shows the inclination of the towers with respect to the vertical direction. The verticalization procedure brought both point clouds' axes to vertical position and shifted the point clouds to the origin of the coordinate system. As a result, successive levels of the wooden tower of St. Bravo church obtained concentric positions after implementation of the multi-modal axis of symmetry (Fig. 6d).

3.2.2. Regular polygon estimation

Regular polygons have equal angles between successive vertices. This property was used in the partitioning of the verticalized point clouds, which are shifted to the origin of the coordinate system. As a result, the directions of the polygon edges (cf. Fig. 4) depend only on the vertices coordinates. Also, the verticalization procedure eliminates the z-coordinates impact on the direction calculation. Values of the edge vertices directions $dir^{n,i}$ were obtained using the formula $dir^{n,i} = atan\,2(\boldsymbol{D}_x^{n,i}, \boldsymbol{D}_y^{n,i})$ where $\boldsymbol{D}^{n,i}$ denotes the i-th vertex of the n-th verticalized point cloud cross-section (Fig. 7).

This study fits two (squared structure) or four (octagonal structure) straight lines to a set of points. Each line estimate contains two opposite vertices. For this purpose, it is most convenient to use the ordinary least-square (OLS) where the key is to maintain fixed angles of 90° and 45° between intersecting lines for square and octagon, respectively. Additionally, all lines must theoretically intersect at one point. For this reason, lines are fitted using the conditional criterion of the objective function of the least squares method (cf. [41]):

$$\varphi(\boldsymbol{y}, d\boldsymbol{x}) = \boldsymbol{v}^T\boldsymbol{v} + \varepsilon\boldsymbol{\kappa}^T(\boldsymbol{B}d\boldsymbol{x}+\Delta) = \underset{d\boldsymbol{x}}{min}, \tag{14}$$

where $\boldsymbol{v} \in R^n$ denotes the vector of the theoretical corrections with the expected value $E(\boldsymbol{v}) = \boldsymbol{0}$ such that $\boldsymbol{v} = \boldsymbol{A}d\boldsymbol{x} + \boldsymbol{L}$, $d\boldsymbol{x} \in R^r$ denotes the vector of increments to the vector of approximate parameters $\boldsymbol{x}^0$ such that $\boldsymbol{x} = \boldsymbol{x}^0 + d\boldsymbol{x}$, $\boldsymbol{A} \in R^{n,r}$ is a known matrix of coefficients such that rank$(\mathbf{A}) = r$. The term $\boldsymbol{L} = \boldsymbol{y}^0 - \boldsymbol{y} \in R^n$ denotes a vector of measured quantities, where $\boldsymbol{y} \in R^n$, and $\boldsymbol{y}^0 \in R^n$ denote vectors of approximate measurement results determined from the basis of approximate values of the parameters. $\boldsymbol{B} \in R^{w,r}$ denotes the matrix of the conditional equations binding the parameter vector, $\Delta \in R^w$ is the conditional values vector, corresponding to the terms $\boldsymbol{B}$ and $d\boldsymbol{x}$. In addition, $\boldsymbol{\kappa} \in R^w$ denotes the vector of Lagrange multipliers, and ε denotes a coefficient with arbitrary values. The solution of the optimization criterion given by Eq. (14) is the vector:

$$d\widehat{\boldsymbol{x}} = -\left(\boldsymbol{A}^T\boldsymbol{A}\right)^{-1}\left(\boldsymbol{A}^T\boldsymbol{L} - \boldsymbol{B}^T\widehat{\boldsymbol{\kappa}}\right), \tag{15}$$

where $\widehat{\boldsymbol{\kappa}} = -[\boldsymbol{B}(\boldsymbol{A}^T\boldsymbol{A})^{-1}\boldsymbol{B}^T]^{-1}[\Delta - \boldsymbol{B}(\boldsymbol{A}^T\boldsymbol{A})^{-1}\boldsymbol{A}^T\boldsymbol{L}]$. Based on Eq. (15), the vector $\widehat{\boldsymbol{x}} = \boldsymbol{x}^0 + d\widehat{\boldsymbol{x}}$ is determined, which includes the estimated values of the directional coefficients of all analyzed lines in 2D space.

The values of matrices Δ and $\boldsymbol{B}$ depend on adopted conditions binding the determined parameters $\boldsymbol{x}$. In the square variant, the terms $\boldsymbol{B}$ and Δ contain one condition that the straight lines ℓ_1 and ℓ_3 intersect at right angle. In the octagonal variant, the terms $\boldsymbol{B}$ and Δ represent 7 conditions: four equations concerning the course of the lines ℓ_1, ℓ_2, ℓ_3, and ℓ_4 through the origin point, two equations fixing the 45° intersection angle between the pair of lines ℓ_1 and ℓ_2, and ℓ_3 and ℓ_4. The last condition defines that the lines ℓ_1 and ℓ_3 intersect at right angle.

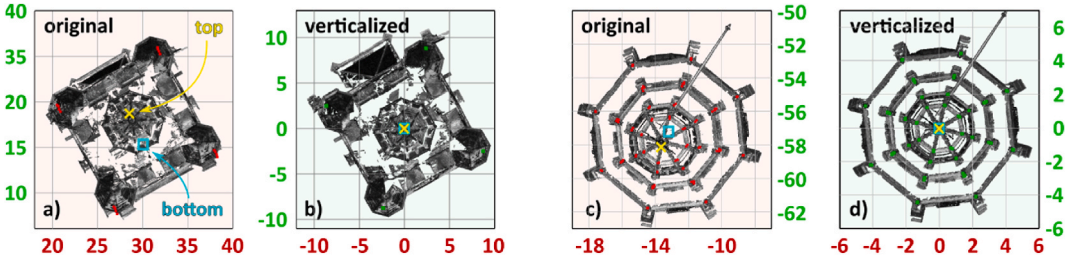

Fig. 6. Verticalization of the Delft (left two panels) and Haarlem St. Bavo (right two panels) towers' point clouds and their polygon vertices.

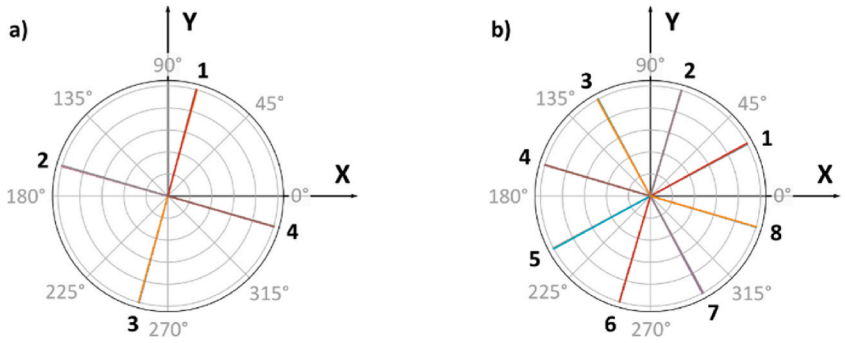

Fig. 7. Four (a) and eight (b) adjusted directions of the Delft and Haarlem St. Bavo towers, respectively.

The adjusted directions $\widehat{\mathbf{X}}_{dir}$ are obtained from the adjusted values of the diagonal line slopes $d\hat{x}$. The adjusted values of the directions $\widehat{dir}^{\,i}$ meet the condition of the fixed angle related to the given regular polygon in the original point clouds local coordinate systems (cf. Fig. 6).

3.2.3. World orientation and partitioning

The last factor preceding the verticalized point cloud partitioning is the orientation of the axes of the local registration coordinate system (cf. Fig. 6) to the four directions of the world, denoted cardinal orientation. Used tower point clouds were not geo-referenced, so their orientation did not represent the world coordinate system. The point clouds were rotated to achieve that the four 90°-spaced towers' faces were perpendicular to the direction of the axis of the cardinal system as obtained by Eq. (16):

$$\mathbf{P}'' = \mathbf{R}_Z\left(\widehat{dir}^{\,i=1} - \pi(1+2c)\,/\,\mathscr{N}\right)\mathbf{P}', \tag{16}$$

where $\mathbf{P}''$ denotes the verticalized point from the cloud with cardinal orientation, and c denotes the empirical parameter defining the number of $2\pi/\mathscr{N}$ point cloud rotations. $\mathscr{N}$ denotes the number of angles in the square or octagonal polygon.

Medieval churches were built with the central nave facing the east-west direction. The churches in Delft and Haarlem do not fully comply with this condition. Therefore, in the process of cardinal orientation, the condition of the perpendicularity of the walls and the coordinate system axes was maintained. The red frames in Fig. 8 indicate the location and the orientation of the two analyzed towers. Partitioning of a verticalized point cloud into $\mathscr{N}$ parts related to $\mathscr{N}$ polygon angles consists of assigning a parameter $m \in \langle 0, \mathscr{N}-1\rangle$ to each point based on its radial position.

The point cloud after the cardinal orientation represents the faces of the towers according to the real-world position of both objects. The partitioning procedure assigned to each point a parameter m increasing counter-clockwise from the eastern direction of the X-axis (cf. Fig. 8). The Delft Old Church tower point cloud with a square cross-section was divided into $\mathscr{N} = 4$ parts. For the octagonal tower in Haarlem St. Bavo Church $\mathscr{N} = 8$ subsets were created. Each partition was considered separately and PCSE-projected according to the order indicated by the face parameter m using the prismatic point cloud spatial expansion formulas presented in the next subsection.

3.3. Prismatic point cloud spatial expansion (Stage III)

This section describes the expansion of a point cloud of a prismatic historic tower. The expansion is an alternative form of geometry presentation that enhances the asymmetry assessment. The obligatory procedures preceding the transformation are verticalization, cardinal orientation, and point cloud partitioning. The first two operations eliminate the influence of the inclination and modularity of the symmetry axis of the object. The third operation divides the point cloud according to the radial criterion of the cardinal directions of the world. The introduced division causes the occurrence of discontinuities in the expansion, which is the difference between the cylindrical and prismatic variants of the PCSE method.

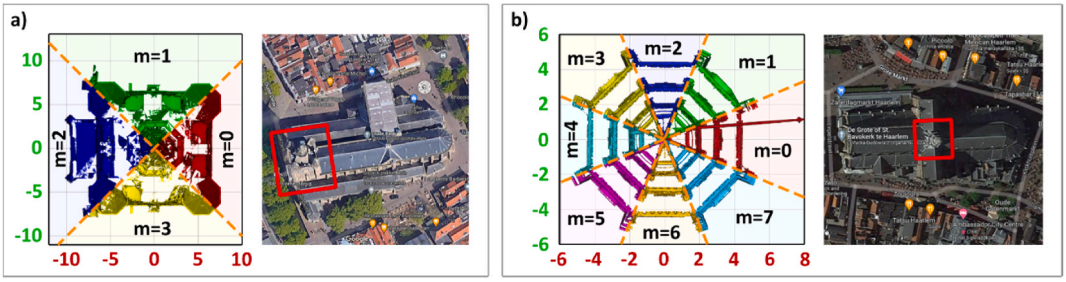

Fig. 8. Partitioned verticalized point clouds of the Delft Old (a) and Haarlem St. Bavo (b) church towers.

Both the symmetry axis and the size of the reference solid need to be defined to create the expansion. In case of prismatic PCSE, the partitioning procedure introduces a separate projection of each of the $\mathcal{N}$ point cloud partitions implying a local quasi-continuity in each partition. Also, stretching and contraction factors do not affect the point cloud. The depth parameter expresses the topology of the points related to the face of the reference prism. To avoid overlap of the projections of individual PCSE sections, the lengths of the sides of the prism bases were defined based on the dimensions of circles circumscribing the objects' point clouds. Circle radii are $r = 11m$ for the Delft Old Church tower and $r = 6m$ for the Haarlem St. Bavo Church tower were obtained by estimating the distance to the axis of the points most eccentric from the cloud (Fig. 9).

The polygons marked in red represent the basis of the two towers' reference prisms. Side length d and side-to-center height h defined by the circle of radius r circumscribing the polygon were obtained by formulas:

$$d = 2r \bullet sin(\pi / \mathcal{N}), \tag{17}$$

$$h = r \bullet cos(\pi / \mathcal{N}). \tag{18}$$

The prismatic point cloud spatial expansion function takes the form:

$$\boldsymbol{P}_{PCSE} = \boldsymbol{R}_X(\pi/2)\boldsymbol{R}_Z(\pi/2 + 2m \bullet \pi/\mathcal{N})\boldsymbol{P}'' + [\,d(2\mathcal{N}+1)/2 \quad 0 \quad -h\,]^T. \tag{19}$$

4. Results

This section is divided into two major parts for the Delft Old Church tower and the Haarlem St. Bavo church tower, which consists of the parameters estimation results and the obtained point cloud spatial expansions. The asymmetry assessment includes the geometry of the wall and facades planes, the location of the tower stories levels, the symmetry of the arrangement of the turrets (cf. Fig. 1), and the course of the multi-modal symmetry axis. The developed solutions were not included in the Case study and Methods section but presented in Sections 4.1 and 4.2 with the analysis results.

4.1. The Delft Old Church tower

The determination of the objects' symmetry axes is based on the estimated cross-section centers. The shape of the tower and the usage of TLS technology for data acquisition resulted in an incomplete representation of the surfaces of the structures. This factor affected most of the lower parts of the tower adjacent to the roof due to occlusions and obstruction. As a result, the selection of cross-sections depended on the completeness of the point cloud on all sides of the towers. Eleven cross-sections of the Delft Old Church tower were extracted (c.f. Fig. 3). RANSAC was used to eliminate outliers not belonging to wall surface and the course of the three-dimensional axes was determined by PCA (c.f. Section 3). In RANSAC the parameters of sampling resolution of 0.1 m, max normal deviation of 25.0°, max distance to plane of 0.05 m, and overlooking probability of 0.01 were used. The calculation was performed in CloudCompare software [42].

A notable feature of the Delft Old Church tower, apart from the inclination axis from the vertical, is the asymmetric position of the subsequent tower floors. The quality of axis estimation was validated with a T-test [43,44] based on the χ^2 distribution. In the calculation, the residuals values of the points that are distances of points to the estimated axis line and the values of variance were used. The confidence level n_T was defined by the number of points used in the estimation and the number of two points necessary to define a line in $\mathscr{R}^3$. The estimated parameters of the axis were considered acceptable when the residuals fulfilled the boundary conditions implied from the χ^2, that is when the test statistic as built from the residuals had a value below the critical value following from the distribution. The obtained value was 15.4, meeting the criteria of the T-test for $n_T = 9$, and the confidence level $\alpha_T = 0.05$.

The axis of symmetry of the Delft Old Church tower is inclined from the vertical by 2.6°. The projections of the lowest and highest points on the estimated inclined axis of symmetry were determined. Location of both points resulted from coverage of the point cloud that did not represent the full extent of the church tower. Hence, the lowest point is not related to the ground level, but to the height of the lowest cross-section. The calculated displacement of the three-dimensional axis equaled 3.73 m, and 81.36 m in the horizontal and

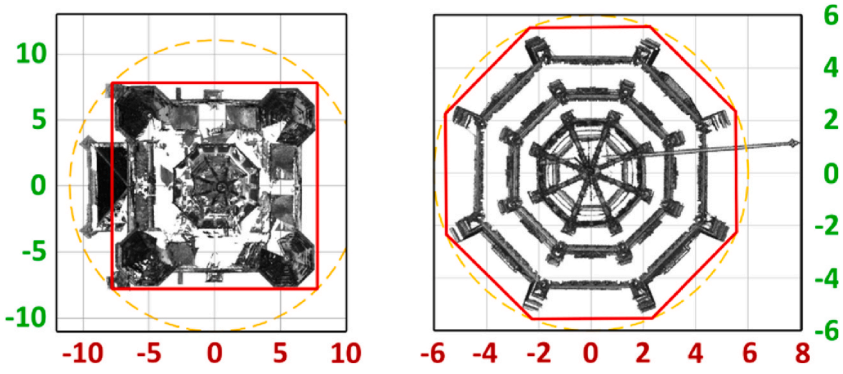

Fig. 9. Reference polygons fitted in circles circumscribing the cardinally oriented point clouds.

vertical planes, respectively. Both distances were calculated based on coordinates of projections of the lowest and the highest points from the cloud on the estimated axis. The original point cloud horizontal plane direction was 114.5° relative to the X-axis. Taking into account the cardinal orientation parameters, the corrected direction equaled 174.7° relative to the normal direction of the eastern wall of the tower (cf. Fig. 8a), which corresponds to the inclination of the tower towards the west.

With the symmetry axes determined, the verticalization procedure (Eq. (13)) was carried out to eliminate the factor of the tower' inclination. The horizontal coordinates of the cross-section vertices, after the reverse transformation (Eq. (9)) to the original point cloud system, were also verticalized. The point clouds partitioning was carried out using the horizontal coordinates of the cross-section vertices. Position of vertices of 11 point cloud cross-sections were included in four sets with vertices directions (cf. Fig. 4). The adjustment procedure (Eqs. (14) and (15)) resulted in the determination of the directions estimators meeting the condition of a fixed central angle between vertices equal to 90°. On this stage, the point cloud maintained the initial orientation of the point cloud that did not meet the real-world directions criterion.

The value of the first adjusted direction was used in the cardinal orientation of the verticalized point cloud. The value of the empirical parameter c defining the number of additional rotations of 90° resulted from the orientation of the verticalized point clouds in the local coordinate system. After the cardinal orientation of the point clouds, the partitioning procedure was introduced. Next, the partitioning parameter m was used in the prismatic spatial expansion of the point cloud of the tower. The result of the application of the PCSE method and selected metric parameters of the Delft tower are shown in Fig. 10.

The verticalized point cloud with $\mathcal{N} = 4$ partitions was projected in an alternative form that enables the tower's geometry assessment in relation to the estimated axis of symmetry. The point cloud partitions shown in Fig. 8 were marked according to the corresponding values of the parameter m. The PCSE depth parameter introduces a new geometrical measure unavailable in either the original or the verticalized point clouds. This measure is the distance of the points from the adjacent reference prism face. The positive and negative values of the depth parameter indicate the topology of points and the reference prism. Positive values represent historic tower elements that are located outside the faces' surfaces, e.g. the Delft Old Church tower entrance portal. Negative values of the depth parameter mean that the points are located inside the solid, below the prism faces.

The elimination of the inclination factor enabled conducting the towers' asymmetry analyses. For example, in the left panel of Fig. 10 presenting the expansion of the point cloud of the Delft Old Church tower, the eccentric position of the central spire of the tower is visible. The comparison of the distance between the reference prism face, the symmetry axis, and the depth parameter read from the expansion, indicates that the central spire is separated 0.51 m from the axis of symmetry in the east direction. The shift value was obtained from comparison of the position of the main tower axis and the spire axis.

4.1.1. Walls deformations

The RANSAC filtering (c.f. Section 3) resulted in subsets of points of planes (Fig. 3). Each subset had a separate depth parameter range defining the geometry of a single wall panel with respect to the faces of the reference prism (Fig. 11).

The PCSE's depth parameter represents the uniform walls asymmetry related to the reference prism sides. The largest deformations were obtained on the western wall ($m = 2$). The magnitude of deformations at storey 1 and 2 increases with the height. In the total height range of 25 m, the depth parameter increased by 0.3 m. The course of the remaining walls was more regular. To define the degree of asymmetry of individual wall panels, three parameters were calculated. The coordinates of the normal vectors $\boldsymbol{V}_{PCA}^{norm}$ were determined using PCA. The values of the slopes in the upwards (s) and transverse (cs) directions were also obtained. The geometry of

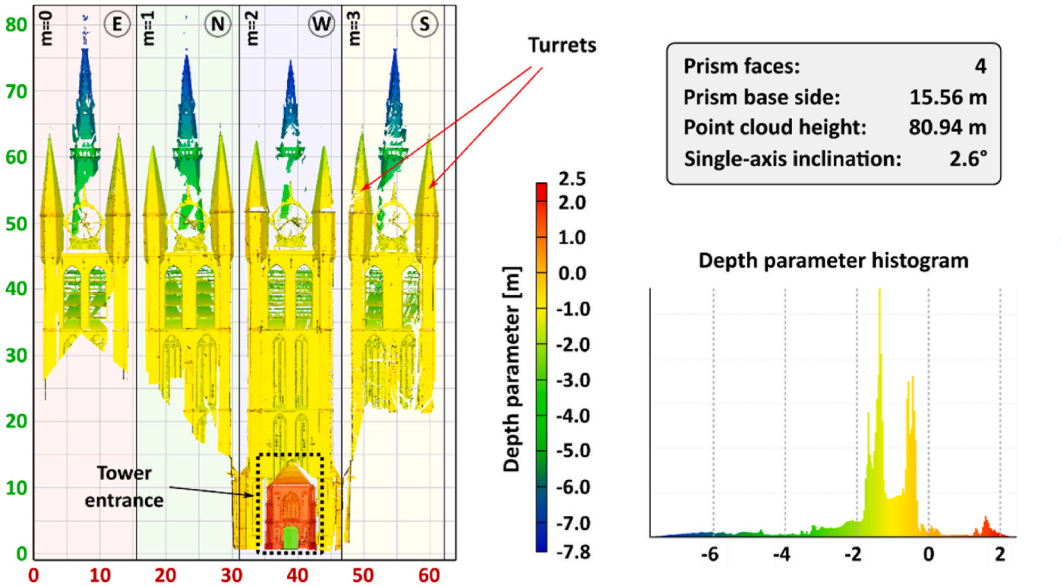

Fig. 10. Top orthogonal view of the prism PCSE (left panel) and key metrics with depth parameter histogram (right panel) of the Delft Old Church tower.

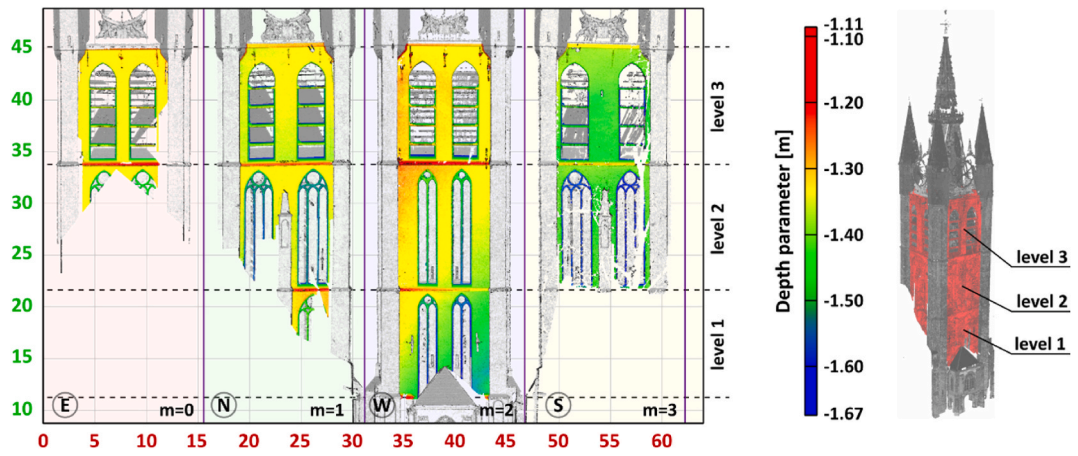

Fig. 11. The Delft Old Church tower walls deformations.

wall point clouds, fitted planes, and the slopes vectors are presented in Fig. 12.

The analysis was carried out in the expanded point cloud. The vectors $\boldsymbol{V}_{PCA}^{norm}$ align towards the PCSE system Z-axis (cf. Fig. 11). The deviation of the vector from the normal direction of the reference prism face was calculated using the formula:

$$i = acos\left(\left(\boldsymbol{V}_{PCA\,x}^{norm\,2} + \boldsymbol{V}_{PCA\,y}^{norm\,2}\right) \Big/ \left|\boldsymbol{V}_{PCA}^{norm}\right|\right). \tag{20}$$

The direction α_i of the vector $\boldsymbol{V}_{PCA}^{norm}$ in the PCSE XY plane was determined as follows:

$$\alpha_i = atan\left(\boldsymbol{V}_{PCA}^{norm}y \Big/ \boldsymbol{V}_{PCA}^{norm}x\right). \tag{21}$$

The vectors $\boldsymbol{V}^{s}$ and $\boldsymbol{V}^{cs}$ indicating the directions of two slopes were obtained from the vector products:

$$\boldsymbol{V}^{s} = \boldsymbol{V}_{PCA}^{norm} \times [1 \quad 0 \quad 0]^{T}, \tag{22}$$

$$\boldsymbol{V}^{cs} = \boldsymbol{V}_{norm}^{PCA} \times \boldsymbol{V}^{s}, \tag{23}$$

The percentage values of slopes in the upwards direction (s) and in the transverse direction (cs) were determined using the formulas:

$$s = \boldsymbol{V}_{z}^{s} \Big/ \boldsymbol{V}_{y}^{s} \bullet 100\%, \tag{24}$$

$$cs = sig\left(\boldsymbol{V}_{PCA}^{norm}x\right) \frac{\boldsymbol{V}_{z}^{cs}}{\sqrt{\left(\boldsymbol{V}_{x}^{s}\right)^{2} + \left(\boldsymbol{V}_{y}^{s}\right)^{2}}} \bullet 100\%, \tag{25}$$

where *sig* denotes the signum function.

The results of the analysis of the asymmetry of the wall panels of the Delft Old Church tower are presented in Table 1.

The western wall panels ($m = 2$) on levels 1 and 2 (cf. Fig. 11) show higher values of asymmetry parameters than the other panels. Normal vectors deviated by 0.7° and 1.1° from the reference face normals, which resulted in the highest wall slope values of 0.79% and 1.21%, respectively. A significantly greater slope s was also obtained on the southern wall ($m = 3$). In the case of a cross-slopes cs, the eastern wall panels also obtained the highest values of 0.95% and 1.49% for levels 1 and 2, respectively. The anomalous values of the

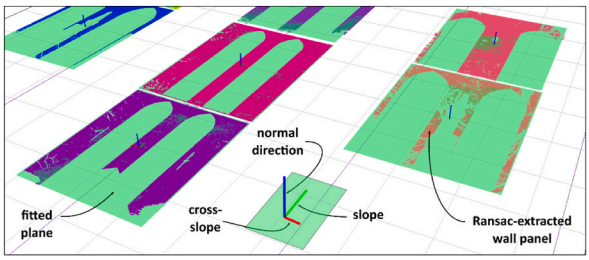

Fig. 12. Walls asymmetry parameters.

Table 1
The Delft Old Church tower walls asymmetry parameters values.

Wall panel (direction, m, level)	Vector on-plane direction [°]	Vector normal deviaton [°]	Slope [%]	Cross-slope [%]	Mean DP (*) [m]	StDev DP (*) [m]
E, 0, 3	−153.4	0.3	0.25	**−0.51**	−1.34	0.02
N, 1, 3	−113.7	0.2	0.29	−0.13	−1.37	0.01
W, 2, 3	23.5	0.3	−0.24	**0.56**	−1.32	0.02
S, 3, 3	−79.6	0.3	**0.58**	0.11	−1.44	0.02
N, 1, 2	−101.3	0.2	0.27	−0.05	−1.37	0.01
W, 2, 2	−39.9	**0.7**	**0.79**	**0.95**	−1.34	**0.04**
S, 3, 2	−88.0	0.1	0.22	0.01	−1.44	0.01
W, 2, 1	−39.0	**1.1**	**1.21**	**1.49**	−1.43	**0.06**

(*) - PCSE depth parameter.

two slopes did not always occur together, as indicated by the values of the panels at level 3 of the tower. The PCSE depth parameter ranges confirmed the formulated conclusions by obtaining over 4 cm standard deviations for the two lower levels of the eastern wall.

4.1.2. *Turrets geometry*

A third analysis of the asymmetry of the Delft Old Church tower is related to the arrangement of the four octagonal turrets (small side-towers) located at the top of the structure (cf. Fig. 1). To obtain a continuous representation of the tower turrets required an independent modified spatial expansion. The verticalized point cloud, after applying the cardinal orientation procedure (Eq. (16)), obtained the position of the tower walls perpendicular to the coordinate system axes (cf. Fig. 6). Introduction of an additional rotation around the Z-axis results in a change in the position of the turrets, which obtain the projections not at the edges, but in the center of the partitions:

$$\mathbf{P}'' = \mathbf{R}_Z(\pi/4)\mathbf{R}_Z\left(\widehat{dir}^{\,i=1} - \pi(1+2c)/4\right)\mathbf{P}'. \tag{26}$$

For each of the turrets, the cross-sectional algorithm of Section 2.1 was used to estimate the parameters of their axes of symmetry. The problem was the lack of one of the sides of the octagonal cross-section in the point cloud caused by the connection of the turrets to the tower. This resulted in a reduction in the number of vertices and diagonals used to determine the center of the cross-section (Eq. (8)). Four obtained turret axes were defined by estimators of points and direction vectors of the axes (Eq. (10)). To assess the objects' asymmetry, the PCSE coordinates of the top points of the turret spires were calculated. The scaling parameter t (Eq. (11)) values were defined as temporary points and the coordinates of their projections on the axes were obtained. The point cloud expansion with the additional rotation applied, is presented in Fig. 13.

Assessment of the asymmetry of the turrets was carried out in two stages. First, the direction of the Delft Old Church tower symmetry axis and the axes of the four turrets were compared. In the next stage, the asymmetry parameters of the turrets' spire tops were determined. The angles between the verticalized tower axis and turret axes were determined using the formula:

$$\gamma = acos\left(\sqrt{\left(V_x^{PCSE}\right)^2 + \left(V_z^{PCSE}\right)^2} \Big/ \left|V^{PCSE}\right|\right), \tag{27}$$

where V^{PCSE} denotes the turret axis vector.

The spatial distribution of the turrets in the horizontal plane of the verticalized point cloud (Fig. 6) was determined using the values of adjusted directions used in the partitioning procedure:

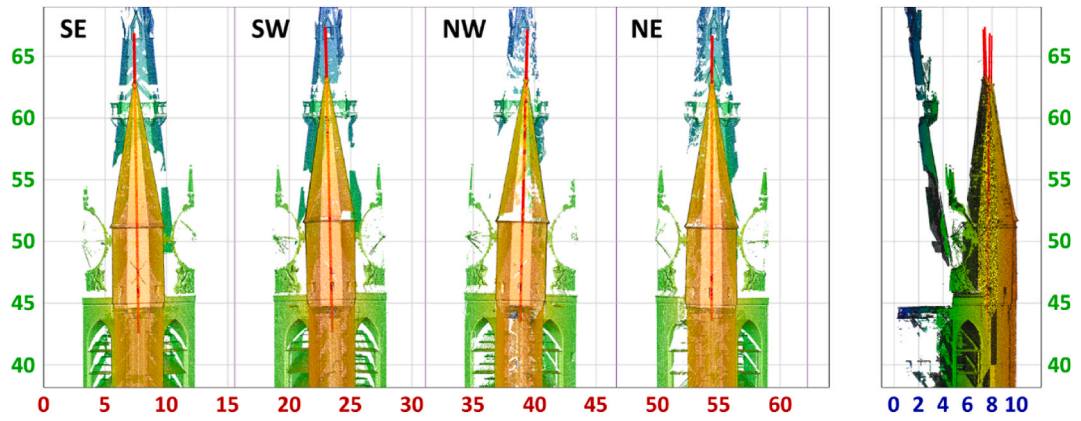

Fig. 13. Delft Old Church turret axes in a top (left panel) and side (right panel) views of the PCSE.

$$d\theta = atan\left(\left(x^{PCSE} - a \bullet (m - 1/2)\right)/h\right). \quad (28)$$

The asymmetry parameters of the turret axes are presented in Table 2.

The analysis showed deviations of all turrets' axes from the direction of the main tower axis exceeding 0.5°. The turrets with the greatest inclination exceeding 2.0° are located on the west side, which is the direction of the leaning of the Delft Old Church tower. The axes deviation of the two turrets implies the smallest values of the depth parameter (Table 2). Hence, the two described turret spire tops are located closest to the tower axis of symmetry. The radial arrangement of the turrets differs significantly from the theoretical shape of the reference prism cross-section directions. Excluding the north-east turret, the radial deviations of the remaining turrets exceeded absolute values of 2.0° (south turrets) and 3.0° (north-west tower).

4.2. The Haarlem St. Bavo Church tower

The methodology used for determining the asymmetry parameters of the Delft Old Church tower was also applied to the facades of the Haarlem St. Bavo Church tower. The main difference was the doubled number of sides in the point cloud cross-sections, which introduced more parameters in the estimation procedures. Twelve cross-sections of the tower point clouds were extracted (c.f. Fig. 3). A gradual deviation of the axes of subsequent levels was observed and taken into account in the object's symmetry axis estimation.

Similarly, to the Delft tower case (c.f. Section 4.1), the quality of the Haarlem tower axis estimation was validated with a T-test. Using all cross-section centers in line fitting, the value of 43.0 was obtained, which did not meet the T-test criterion for $n_T = 10$, which was a premise for the introduction of the multi-modal axis. Hence, three variants of the multi-modal axis configurations were analyzed, including one, two, and three symmetry axes, respectively. Levels of the Haarlem St. Bavo Church tower and the single-axis residuals are presented in Fig. 14.

The first variant presents one uniform axis for the entire object (left panel of the figure). The second variant involves two axes, the first assigned to lower level 1 of the tower, and the second assigned to the higher tower levels 2 to 4 (middle panel). The value of the T-test for the axis of level 1 of the tower at $n_T = 2$ was 7.7, which passed the T-test at the confidence level $\alpha_T = 0.01$. The test was not passed for the subsequent levels 2 to 4, with a value of 26.0 with $n_T = 6$. Therefore, additional segmentation of the axis of symmetry of the upper levels 2 to 4 was performed.

The last third variant introduced separate axes of symmetry for levels 1 and 2 and a joint axis for levels 3 and 4. The T-test for the axis fitted to the cross-section centers at level 2 showed a value of 7.0 not exceeding the boundary value for $n_T = 2$ with a confidence level $\alpha_T = 0.025$. In the case of the axis of the two highest levels, the test value was 7.5, which met the criteria for $n_T = 2$ and for the confidence level $\alpha_T = 0.01$. The obtained T-test validation confirmed the validity of the introduction of the modular axis of symmetry consisting of three segments for the Haarlem St. Bavo Church tower. The point cloud verticalization procedure (Eq. (13)) eliminated the influence of the changing course of the multi-modal axis. Next, the directions obtained in the adjustment procedure resulted in meeting the condition of the fixed central angle between the vertices equal to 45°.

The detailed analysis of the axis course is presented in Section 4.2.1 and the analysis of the geometry of the tower facades is described in Subsection 4.2.2. The result of the PCSE method application and selected metric parameters of the Haarlem tower are presented in Fig. 15. The value of the used empirical parameter defining the number of additional rotations of 45° (c.f. Section 3.2.3) equaled $c = 1$.

4.2.1. Multi-module axis torsion

The axis of symmetry of the wooden tower of Haarlem St. Bavo Church was not rectilinear. The analysis of the axis course implied assigning four separate modules of axis of symmetry for four levels of the tower (cf. Fig. 14). Each module of the axis was attributed by the directional (Eq. (10)) and the boundary levels displacement (Eq. (12)) vectors. The verticalization procedure eliminated the factor of multi-modal axis inclination and modified the structure of the original point cloud to the form applicable for the PCSE method processing. Fig. 16 presents the torsion parameters of three consecutive level axes.

The height of the boundary planes was determined based on the tower's outer edges level located below the stories railings. The coordinates of the planes' normal vectors (blue axis) coinciding with the directions of the multi-modal axis of symmetry were obtained as described in Section 3. The orientation of two other vectors indicating the plane slopes was defined using Eq. 24 and 25. The green axis vectors define the slope of the consecutive story planes and the direction of inclination of the normal-to-plane vectors. The left panel of Fig. 16 presents the multi-modal axis torsion components in the orthogonal top view. Values of the parameters are presented in Table 3.

It should be noted that, as the original non-processed point cloud was used in the analysis, the presented angular values were related to the direction of the X-axis of the local coordinate system. The comparison of the values to four directions of the world is achieved by reducing the presented values by the cardinal orientation angle which equaled 51.7°. By applying this correction, all angles obtain values in relation to the X-axis, which is perpendicular to the eastern facade of the tower (cf. Fig. 8).

Table 2
Delft Old Church tower turrets asymmetry parameters.

Turret (direction, m)	Axis deviation [°]	Spire top depth parameter [m]	Spire radial deviation [°]
SE, 0	1.0	−0.25	**−2.6**
SW, 1	**2.1**	**−0.48**	**−2.1**
NW, 2	**2.1**	**−0.63**	**3.1**
NE, 3	0.5	−0.07	0.1

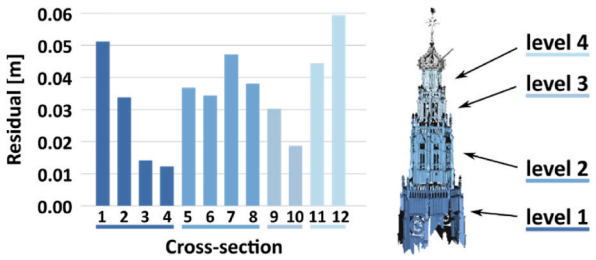

Fig. 14. Residuals of the center points used in the Haarlem St. Bavo Church tower axis estimation.

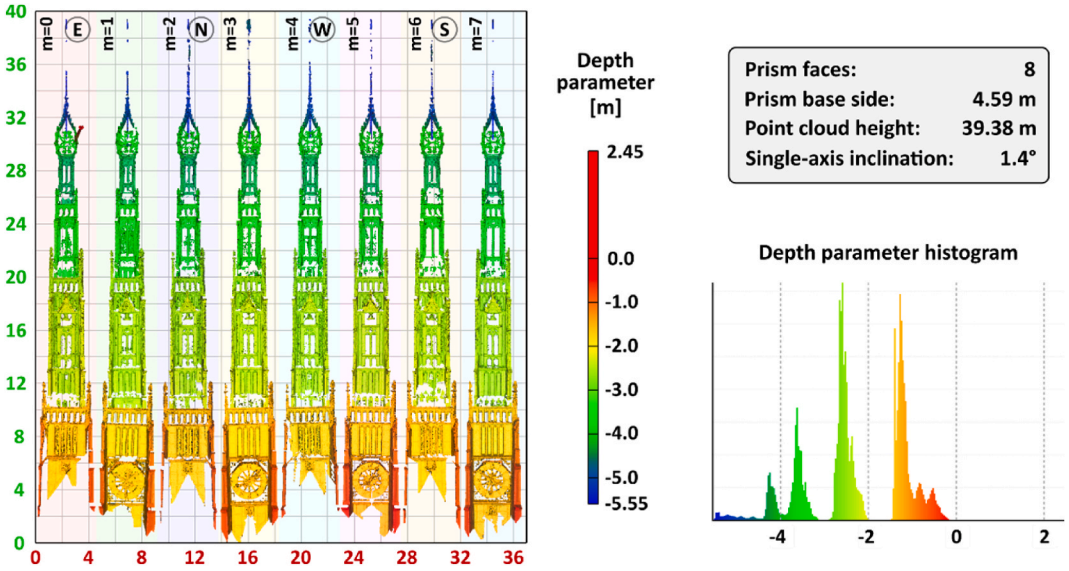

Fig. 15. Top orthogonal view of the prism PCSE (left panel) and key metrics with depth parameter histogram (right panel) of the Haarlem St. Bavo Church tower.

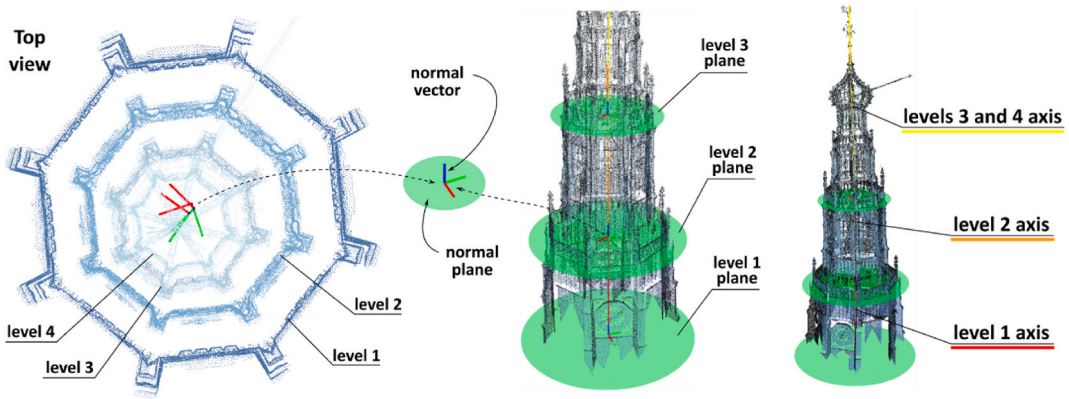

Fig. 16. The Haarlem tower multi-axis torsion.

Table 3
Haarlem St. Bavo Church tower multi-modal axis radial geometry in the original point cloud coordinate system.

Level	Vn = [x, y, z]^T [m]			Level height [m]	dHz [m]	dV [m]	Inclination [°]	Direction [°]
1	0.01	−0.02	1.00	8.94	0.16	8.94	1.76%	−71.3
2	−0.02	−0.02	1.00	9.87	0.22	9.86	2.18%	−134.9
3–4	−0.03	−0.02	1.00	20.59	0.74	20.57	3.58%	−136.0

For the first level of the tower a different inclination direction was estimated than for the higher levels where the gradual impact of the tower multi-modal axis torsion was increasing. The axis module deviation values increased from 2.2° for the second level to 3.6° for the higher levels (Table 3). Values of the linear error resulting from the axis modules' inclination were presented in Table 4.

The coordinates of the points of intersection of the multi-modal axis segments at the boundary levels were presented in the first two rows of the table. The vector of the axis modules shift was presented in the third row. The last rows of the table present the length and the XY plane direction of the shift vectors. The graphical interpretation of the multi-modal axis course is presented in Fig. 17.

The figure contains a plan view of the XY plane (left panel) and a side view of the XZ plane (right panel). The multi-modal axis segments are presented in brown, red, orange, and yellow colors accordingly to the tower levels. The shift vectors are presented in black on the green rectangles denoting the boundary planes from Fig. 16. The last element of the figure are cumulative distances and angles between the extremal points from the cloud projected on the multi-modal axis. The module of the three-dimensional vector connecting the two indicated points equaled 39.40 m. In two orthogonal projections on the XY and XZ planes that distance corresponded to 1.04 m and 39.38 m, respectively. The analysis of the parameters of the tower axis torsion confirmed the validity of adopting the methodology of segmentation of the axis according to the successive levels of the tower. Taking into account the value of the cardinal orientation angle, the western direction of the tower inclination was indicated.

4.2.2. Walls deformations

The wooden octagonal tower was divided into four levels (upper-right panel of Fig. 16). The first three levels have observation decks with railings at the tops. The walls of the tower consist of wooden facades. The PCSE depth parameter was used in the assessment of the facades' asymmetry with respect to the reference prism of the tower. The novel factor is to analyze facades' geometry in relation to the inclined axis of symmetry. An example of three facades located on level two is presented in Fig. 18.

The figure presents parts of eight expansion partitions in orthogonal top view. The uniform scale of the depth parameter describes the regularity of the facade elements' distribution. The verticalized point cloud introduces uniform height values corresponding to the faces of the reference prism. Such an approach is not available in the original point cloud, where only local asymmetry parameters are assessed.

In the first stage of the estimation of asymmetry parameters the RANSAC plane extraction in the expansion point cloud was used. The procedure resulted in extraction of several planes in facades. In the analysis, three variants of the planes' locations on level two of the tower were used (top panel Fig. 19). Each variant represented facades on one of three types of facades on the second level of the Haarlem tower (cf. right panel Fig. 18).

The ranges of the depth parameter in the lower part of Fig. 19 are not uniform and represent the geometry of the individual facades. Introduction of one uniform parameter range would widen its limit values, making the assessment of local asymmetry parameters unclear. The normal vector deviations, slope, and cross-slope values of the facades' planes are presented in Fig. 20. The second level of the tower was divided into three sections labeled 2A, 2B, and 2C (Fig. 19). One scale of the vertical axis was used to present the obtained values of normal vector deviation, slope, and cross-slope parameters jointly.

Normals of facade planes deviate from the planes of reference prism faces on average by 0.9° (level 2A), 0.5° (level 2B), and 0.8° (level 2C). The standard deviation of inclination values of the normal vectors for section 2A of 0.4° was the largest compared to the others. Similarly, level 2B has a value of 0.1° and that of level 2C is 0.2°. No statistically significant correlation between the eight partitions of the cloud of points represented by the parameter m and the deviation of the normal vectors was obtained. It should note that the uncertainty of the results depends on the error of single-point measurement and the point cloud registration errors.

The greatest differentiation in values on the tower second level asymmetry parameters occurred in the facade slopes. Positive values of the parameter indicate the downward inclination of the upper part of the facade surface towards the projected axis of symmetry. Slopes of values not exceeding −0.5% were obtained on the northwest side of the tower ($m = 3,4,5,6$). Negative cross-slope values are the result of the adjustment of directions according to the theoretical octagonal geometry of the cross-section (cf. Fig. 8). The mean values of cross-slopes were −1.08%, −0.78% and, −1.20%, respectively, for levels 2A, 2B and 2C. The transverse direction represented by the facade cross-slopes is similar to the planes of extracted cross-sections of the point cloud (cf. Section 3.1).

5. Conclusions

The paper presents a method for the assessment of historic asymmetry towers. The proposed approach identifies axis segments and indicates the need for the introduction of a multi-module axis according to the geometrical parameters of the object. Validation of the algorithm on the point cloud of the Haarlem St. Bavo Church octagonal tower showed both the several-degree inclinations of the axis modules and the shifts between the consecutive axis segments at the boundary plane levels. The enhanced PCSE-based verticalization procedure was used to mitigate the factors of the axes' inclination and discontinuity factors, and to adjust the original point cloud for the spatial expansion procedure. The PCSE method cannot be used directly in block-based computational analyses to produce numerical models for structures' mechanical monitoring. It can, however, be a valuable tool for the indication of major geometric anomalies.

The current state-of-the-art does not include a method for detailed assessment of the geometrical asymmetry of complex inclined historical towers. Existing approaches focus on the assessment of local deformations on single-wall facades with no reference to the theoretical shape of the structure. Also, in the estimation of the axis of symmetry of towers, in most cases, just linear approximation is considered. To cover those factors different point cloud estimation methods were combined. RANSAC filtration enabled the elimination of outliers from basic towers' wall panels, and the LS estimation with binding conditions was used to indicate the structures axes and planar horizontal direction of the measured point clouds. Finally, the prismatic PCSE was introduced to assess the tower's

Table 4
Haarlem tower multi-modal axis torsion planar geometry.

	Levels 1–2 boundary plane			Levels 2–3 boundary plane		
	x [m]	y [m]	z [m]	x [m]	y [m]	z [m]
Lower-level axis interception	−13.15	−57.36	42.44	−13.28	−57.50	52.31
Upper-level axis interception	−13.13	−57.35	42.44	−13.25	−57.50	52.31
Displacement vector [m]	0.02	0.01	0.00	0.03	0.00	0.00
Distance [m]	0.02			0.03		
Direction [°]	14.3			5.4		

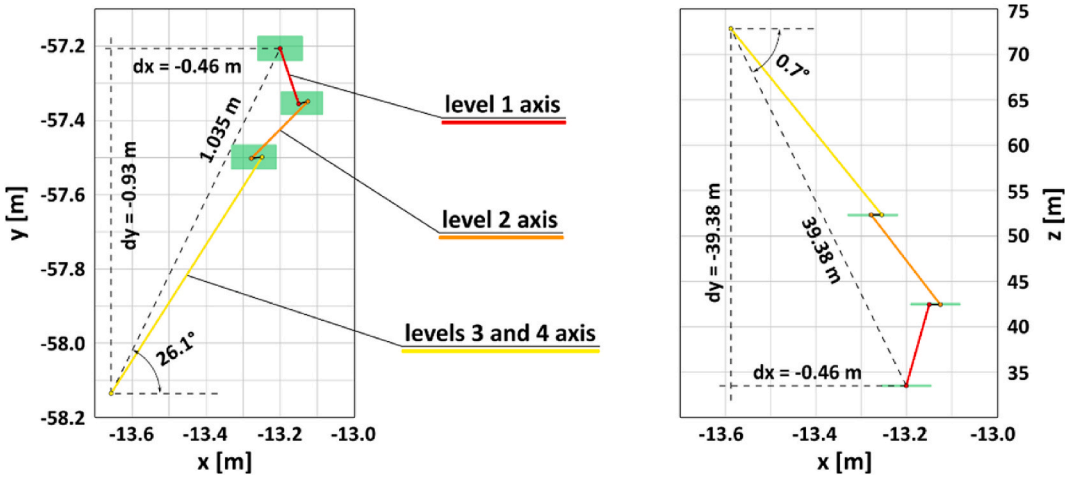

Fig. 17. The Haarlem St. Bavo Church tower multi-module axis course.

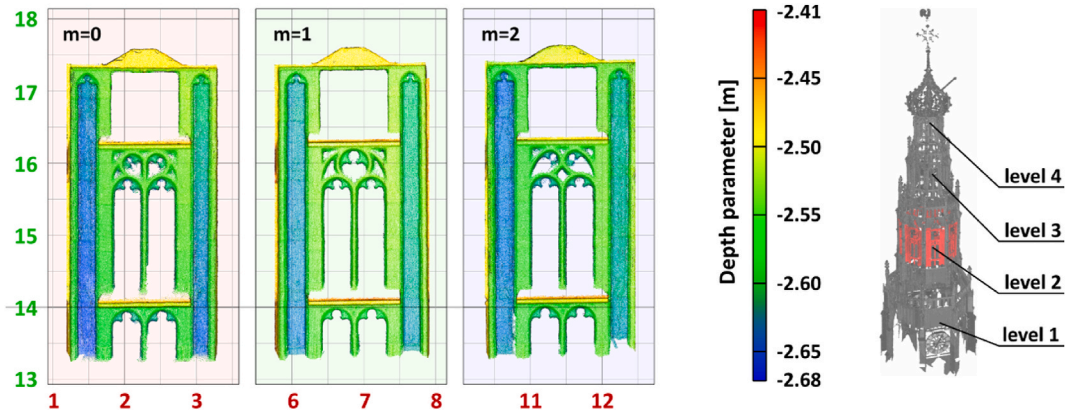

Fig. 18. The Haarlem tower, level two facades geometry.

geometry in an alternative way. The advantage of the proposed method is that using the PCSE depth parameter enabled us to relate the complex multi-sided structure of the towers to the theoretical regular prism of reference which provides a reliable asymmetry description of objects.

The point cloud spatial expansions of the prismatic towers were used to determine asymmetry parameters of facades elements in relation to the tower's central axis. Presentation of the complex geometry of objects in a single spatial view of the expansion enabled assessing the topology of the point cloud and the objects' reference prism shapes. The PCSE depth parameter was used in several assessments, e.g., analysis of the geometry of tower walls and facades, defining the topology of stories planes and tower symmetry axis, and analysis of regularity in the arrangement of architectural features. For each purpose, a separate methodology of using the three-dimensional coordinates of the expansion was developed, resulting in the determination of numerical parameters of the asymmetry.

Several novel factors in the field of remote sensing were introduced in the study. The proposed PCSE-based approach was effective in obtaining the torsion parameters of the multi-module axis of the wooden tower in Haarlem. The RANSAC-processed point cloud was used to determine the three-dimensional parameters of the asymmetry of the walls and facades of the towers. The verticalization

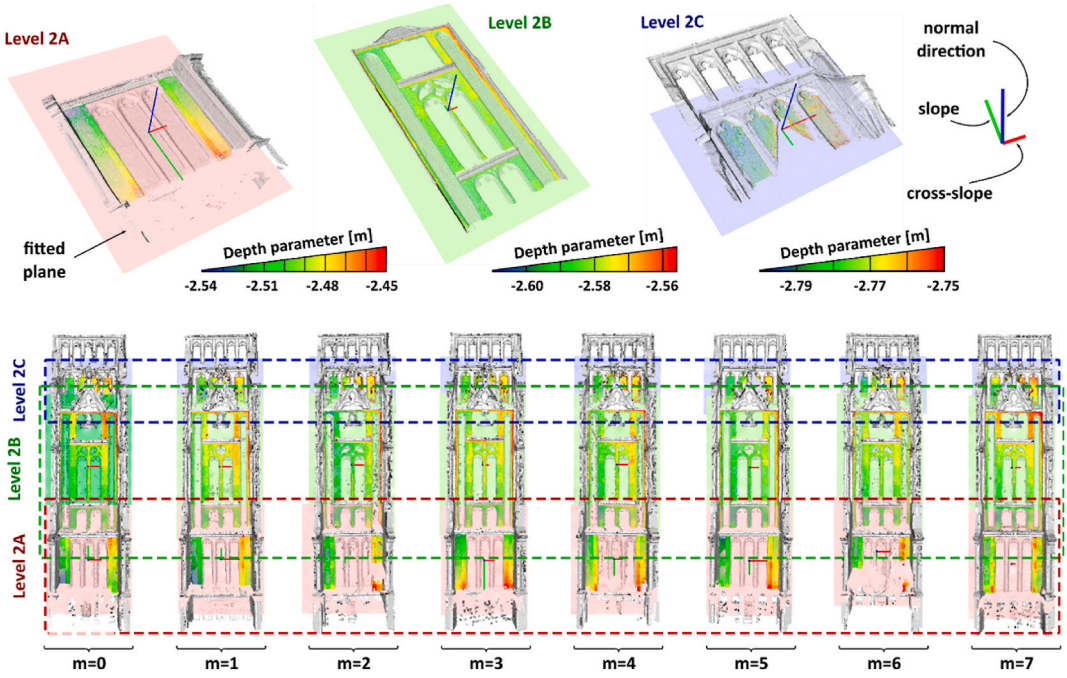

Fig. 19. The Haarlem tower, level two facades', planes asymmetry analysis.

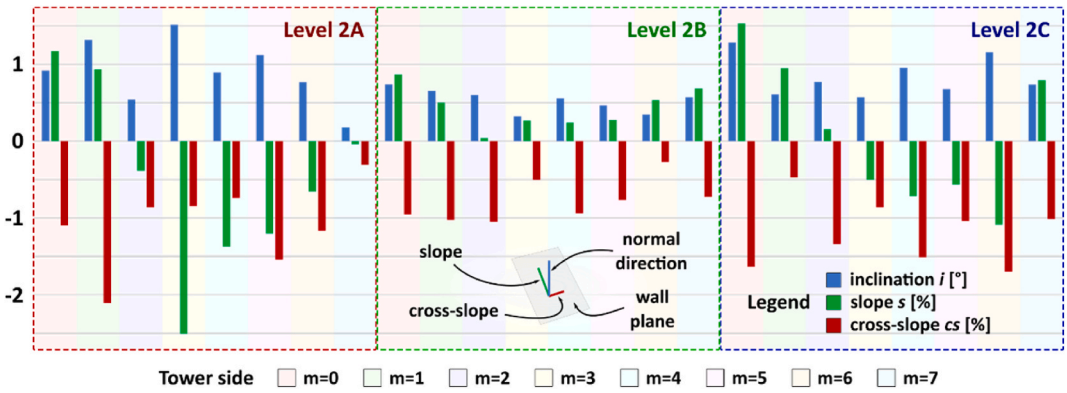

Fig. 20. The Haarlem St. Bavo Church tower level two facades asymmetry parameter values.

procedure analysis enabled the validation of the orthogonality condition between the planes of the tower stories and the multi-modal axis of symmetry. The conducted cross-section directions adjustment was used to assess the radial deviations of architectural details in relation to the theoretical shape of the objects' reference prisms. These parameters can be estimated after applying the prismatic variant of the PCSE method.

Some limitations of the proposed approach need to be addressed. The selection of representative planes from the point cloud to construct the sections involves the elimination of points representing protruding architectural wall features or trees. The RANSAC algorithm enables defining a surface search buffer to identify inlier points. The crucial factor determining the accuracy of the estimation is the quality of the point cloud in terms of both the measurement error and noise intensity. Hence, for each analyzed object, the quality of the data should be inspected first and incorporated accordingly. Another limitation involves non-planar wall shapes, e.g. concave surfaces. In that case, the proposed RANSAC application would not produce valid results. Solving that problem requires the introduction of surfaces with curvatures and is not discussed in this study, but could be implemented in future work using e.g. B-splines. If surfaces from concave wall point clouds would be corrected fitted, that would finally yield the data for the correct estimation of the object's symmetry axis. The finite element method (FEM) can be applied to the original inclined and verticalized point clouds. Also, FEM can be utilized on the PCSE projections of the walls of the tower. In the last case, the introduced alternative representation of the point cloud is expected to enhance the analysis.

Funding

This study was funded by Bekker NAWA grant BPN/BEK/2021/1/00128, and Gdynia Maritime University statutory activities grant WN/2022/PZ/05.

Author statement

PSD: Conceptualization, Methodology, Software, Validation, Formal analysis, Investigation, Data Curation, Writing - Original Draft, Visualization, Project administration, Funding acquisition. MHZ: Methodology, Validation, Formal analysis, Writing - Review & Editing. LTH: Methodology, Validation, Formal analysis, Investigation, Resources, Writing - Review & Editing. RL: Conceptualization, Methodology, Validation, Formal analysis, Investigation, Resources, Writing - Review & Editing, Supervision.

Declaration of competing interest

The authors declare that they have no known competing financial interests or personal relationships that could have appeared to influence the work reported in this paper.

Data availability

Data will be made available on request.

Acknowledgements

The authors thank Dr. AliReza Amiri-Simkooei for the consultation and valuable comments on the adjustment procedure.

References

[1] M. Liu, X. Sun, Y. Wang, Y. Shao, Y. You, Deformation measurement of highway bridge head based on mobile tls data, IEEE Access 8 (2020) 85605–85615, https://doi.org/10.1109/access.2020.2992590.
[2] X. Ji, Z. Miao, R. Kromanis, Vision-based measurements of deformations and cracks for RC structure tests, Eng. Struct. 212 (2020), 110508, https://doi.org/10.1016/j.engstruct.2020.110508.
[3] L. Truong-Hong, R. Lindenbergh, P. Woudenberg, W. Gard, J.W. van de Kuilen, Monitoring deformations of A wooden church tower by laser scanning, in: 12th International Conference on Structural Analysis of Historical Constructions, International Centre for Numerical Methods in Engineering, CIMNE, 2021, pp. 709–721.
[4] N. Squeglia, C. Viggiani, An update on the tower of pisa, in: Geotechnical Engineering for the Preservation of Monuments and Historic Sites III, CRC Press, 2022, pp. 667–676.
[5] S. Ivorra, F.J. Pallarés, J.M. Adam, Masonry bell towers: dynamic considerations, Proceed. Instit.Civ.Eng.Struct. Build. 164 (1) (2011) 3–12, https://doi.org/10.1680/stbu.9.00030.
[6] A.V. Leonov, M.N. Anikushkin, A.V. Ivanov, S.V. Ovcharov, A.E. Bobkov, Y.M. Baturin, Laser scanning and 3D modeling of the Shukhov hyperboloid tower in Moscow, J. Cult. Herit. 16 (4) (2015) 551–559, https://doi.org/10.1016/j.culher.2014.09.014.
[7] R. Kocierz, M. Rębisz, Ł. Ortyl, Measurement point density and measurement methods in determining the geometric imperfections of shell surfaces, Rep. Geodesy Geoinf. 105 (1) (2018) 19–28, https://doi.org/10.2478/rgg-2018-0003.
[8] N. Kassotakis, V. Sarhosis, B. Riveiro, B. Conde, A.M. D'Altri, J. Mills, G. Milani, S. de Miranda, G. Castellazzi, Three-dimensional discrete element modelling of rubble masonry structures from dense point clouds, Autom. ConStruct. 119 (2020), 103365, https://doi.org/10.1016/j.autcon.2020.103365.
[9] C. Wu, Y. Yuan, Y. Tang, B. Tian, Application of terrestrial laser scanning (TLS) in the architecture, engineering and construction (AEC) industry, Sensors 22 (1) (2021) 265, https://doi.org/10.3390/s22010265.
[10] J. Zhou, B. Shi, G. Liu, S. Ju, Accuracy analysis of dam deformation monitoring and correction of refraction with robotic total station, PLoS One 16 (5) (2021), e0251281, https://doi.org/10.1371/journal.pone.0251281.
[11] G. Castellazzi, A.M. D'Altri, G. Bitelli, I. Selvaggi, A. Lambertini, From laser scanning to finite element analysis of complex buildings by using a semi-automatic procedure, Sensors 15 (8) (2015) 18360–18380, https://doi.org/10.3390/s150818360.
[12] F. Esmaeili, H. Ebadi, A. Mohammadzade, M. Saadatseresht, Evaluation of close-range photogrammetric technique for deformation monitoring of large-scale structures: a review, J. Geomat. Sci.Technol. 8 (4) (2019) 41–55.
[13] E. Aldao, H. González-Jorge, J.A. Pérez, Metrological comparison of LiDAR and photogrammetric systems for deformation monitoring of aerospace parts, Measurement 174 (2021), 109037, https://doi.org/10.1016/j.measurement.2021.109037.
[14] G. Vacca, F. Mistretta, F. Stochino, A. Dessi, Terrestrial laser scanner for monitoring the deformations and the damages of buildings, in: 23rd International Archives of the Photogrammetry, Remote Sensing and Spatial Information Sciences Congress, XLI-B5, 2016, pp. 453–460, https://doi.org/10.5194/isprs-archives-XLI-B5-453-2016.
[15] P.S. Dabrowski, C. Specht, Spatial expansion of the symmetrical objects point clouds to the lateral surface of the cylinder – mathematical model, Measurement 134 (2019) 40–47, https://doi.org/10.1016/j.measurement.2018.10.036.
[16] L. Truong-Hong, D.F. Laefer, Validating computational models from laser scanning data for historic facades, J. Test. Eval. 41 (3) (2013).
[17] M. Pereira, A.M. D'Altri, S. de Miranda, B. Glisic, Automatic multi-leaf nonperiodic block-by-block pattern generation and computational analysis of historical masonry structures, Eng. Struct. 283 (2023), 115945, https://doi.org/10.1016/j.engstruct.2023.115945.
[18] G. Bartoli, M. Betti, A.M. Marra, S. Monchetti, On the role played by the openings on the first frequency of historic masonry towers, Bull. Earthq. Eng. 18 (2) (2020) 427–451, https://doi.org/10.1007/s10518-019-00674-5.
[19] G. Standoli, E. Giordano, G. Milani, F. Clementi, Model updating of historical belfries based on oma identification techniques, Int. J. Architect. Herit. 15 (1) (2021) 132–156, 0.1080/15583058.2020.1723735.
[20] A. Ferrante, F. Clementi, G. Milani, Advanced numerical analyses by the Non-Smooth Contact Dynamics method of an ancient masonry bell tower, Math. Methods Appl. Sci. 43 (13) (2020) 7706–7725, https://doi.org/10.1002/mma.6113.
[21] C. Ye, S. Acikgoz, S. Pendrigh, E. Riley, M.J. DeJong, Mapping deformations and inferring movements of masonry arch bridges using point cloud data, Eng. Struct. 173 (2018) 530–545, https://doi.org/10.1016/j.engstruct.2018.06.094.
[22] G. Lenda, J. Siwiec, J. Kudrys, Multi-variant TLS and SfM photogrammetric measurements affected by different factors for determining the surface shape of a thin-walled dome, Sensors 20 (24) (2020) 7095, https://doi.org/10.3390/s20247095.
[23] G. Lenda, M. Ligas, U. Marmol, Determining the shape of the surface of shell structures using splines and alternative methods: Kriging and Fourier series, KSCE J. Civ. Eng. 18 (2) (2014) 625–633, https://doi.org/10.1007/s12205-014-0366-9.

[24] Z. Lu, H. Gong, Q. Jin, Q. Hu, S. Wang, A transmission tower tilt state assessment approach based on dense point cloud from UAV-based LiDAR, Rem. Sens. 14 (2) (2022) 408, https://doi.org/10.3390/rs14020408.
[25] T. Bisschop, Terrestrial Laser Scan Point Cloud of the Oude Kerk, 4TU.ResearchData, Delft, The Netherlands, 2021, https://doi.org/10.4121/14318822.v1.
[26] L. Truong-Hong, R. Lindenbergh, W. Gard, P. Woudenberg, Terrestrial Laser Scan Point Cloud of the Grote of St.-Bavokerk, Haarlem, The Netherlands, 4TU. ResearchData, 2021, https://doi.org/10.4121/14364824.v1.
[27] D.P. Oosterbaan, Nederlands Archief Voor Kerkgeschiedenis (In Dutch), vol. 44, Brill, The Netherlands, 1961, pp. 129–152.
[28] K. Emmens, M. Enderman, R. Van Hemert, R. Kluft, M. Prins-Schimmel, R. Rodenburg, W. Sietsma, E. Vink, De toren van de grote of Sint-Bavokerk (in Dutch), Haarlem: Schuyt, The Netherlands, 2002.
[29] P. Woudenberg, The current state of the St. BavoChurch tower: a verification study and structural analysis of the wooden tower of the St. Bavo church in Haarlem, The Netherlands, master thesis. http://resolver.tudelft.nl/uuid:9ca97b05-5b56-4453-8077-a12a628ab157.
[30] P.S. Dabrowski, Novel PCSE-based approach of inclined structures geometry analysis on the example of the Leaning Tower of Pisa, Measurement 189 (2022), 110462, https://doi.org/10.1016/j.measurement.2021.110462.
[31] P.S. Dąbrowski, M.H. Zienkiewicz, 3D point cloud spatial expansion by total least squares line fitting, Photogramm. Rec. 35 (172) (2020) 509–527, https://doi.org/10.1111/phor.12345.
[32] M.A. Fischler, R.C. Bolles, Random sample consensus: a paradigm for model fitting with applications to image analysis and automated cartography, Commun. ACM 24(6) 381-395.
[33] P.S. Dąbrowski, M.H. Zienkiewicz, Impact of cross-section centers estimation on the accuracy of the point cloud spatial expansion using robust M-estimation and Monte Carlo simulation, Measurement 189 (2022), 110436, https://doi.org/10.1016/j.measurement.2021.110436.
[34] A. Nurunnabi, Y. Sadahiro, R. Lindenbergh, D. Belton, Robust cylinder fitting in laser scanning point cloud data, Measurement 138 (2019) 632–651, https://doi.org/10.1016/j.measurement.2019.01.095.
[35] P.J. Huber, Robust estimation of location parameter, Ann. Math. Stat. 35 (1) (1964) 73–101.
[36] P.J. Rousseeuw, M. Hubert, Robust statistics for outlier detection, Wiley Interdiscipl.Rev.: Data Min. Knowl. Discov. 1 (1) (2011) 73–79, https://doi.org/10.1002/widm.2.
[37] I.N. Bronshtein, K.A. Semendyayev, G. Musiol, H. Mühlig, Handbook of Mathematics, Springer, 2015.
[38] K. Snow, B. Schaffrin, Line fitting in Euclidean 3D space, Studia Geophys. Geod. 60 (2) (2016) 210–227, https://doi.org/10.1007/s11200-015-0246-x.
[39] Z. Wiśniewski, Estimation of parameters in a split functional model of geodetic observations (M split estimation), J. Geodesy 83 (2) (2009) 105–120, https://doi.org/10.1007/s00190-008-0241-x.
[40] M.H. Zienkiewicz, Deformation analysis of geodetic networks by applying msplit estimation with conditions binding the competitive parameters, J. Survey Eng. 145 (2) (2019), 04019001, https://doi.org/10.1061/(ASCE)SU.1943-5428.0000271.
[41] Z. Wiśniewski, Rachunek Wyrównawczy W Geodezji (Z Przykładami), Wydawnictwo Uniwersytetu Warmińsko-Mazurskiego, Olsztyn, Poland, 2016 (in Polish).
[42] D. Girardeau-Montaut, France CloudCompare, EDF R&D Telecom ParisTech 11 (2016).
[43] P.J. Teunissen, Testing Theory an Introduction, VSSD, Delft, 2006.
[44] C.C.J.M. Tiberius, H. van der Marel, R.H.C. Reudink, F.J. van Leijen, Surveying and Mapping, TU Delft OPEN, Delft University of Technology - The Netherlands, 2021.